Supplementary Information (SI) for Journal of Materials Chemistry A.
This journal is © The Royal Society of Chemistry 2026

Supporting Information for

Design narrow band gap small-molecule acceptors with unilateral vinylene π-bridge for high-performance optoelectronic devices

Shuangshuang Li, Tong Liu, Fuzhen Bi, Renqiang Shao, Hongquan Liu*, Jianxiao Wang, Tan Wang, Shuguang Wen*, and Xichang Bao*

Shuangshuang Li, Prof. Hongquan Liu, and Prof. Xichang Bao
College of Materials Science and Engineering, Shandong University of Science and Technology, Qingdao 266590, China, E-mail: liuhq@sdust.edu.cn
Shuangshuang Li, Tong Liu, Dr. Fuzhen Bi, Renqiang Shao, Dr. Jianxiao Wang, Dr. Tan Wang, Dr. Shuguang Wen, and Prof. Xichang Bao
State Key Laboratory of Photoelectric Conversion and Utilization of Solar Energy, Qingdao Institute of Bioenergy and Bioprocess Technology, Chinese Academy of Sciences, Qingdao 266101, China wensg@qibebt.ac.cn; baoxc@qibebt.ac.cn
Dr. Fuzhen Bi, Dr. Jianxiao Wang, Dr. Tan Wang, Dr. Shuguang Wen, and Prof. Xichang Bao
Functional Laboratory of Solar Energy, Shandong Energy Institute; Qingdao New Energy Shandong Laboratory, Qingdao 266101, China

Materials

All reactions were carried out in argon atmosphere. Common solvents were dried and purified by standard procedures. Column chromatography characterizations were performed with the use of silica gel (200-300 mesh). The polymer donor PM6 and compound 1 were purchased from Derthon Materials Co. Ltd. Other materials were purchased from commercial sources and used directly unless stated otherwise.

Synthesis of 12,13-bis(2-ethylhexyl)-3,9-diundecyl-12,13-dihydro-[1,2,5]thiadiazolo[3,4-e]thieno[2'',3'':4',5']thieno[2',3':4,5]pyrrolo[3,2-g]thieno[2',3':4,5]thieno[3,2-b]indole-2,10-dicarbaldehyde(2)

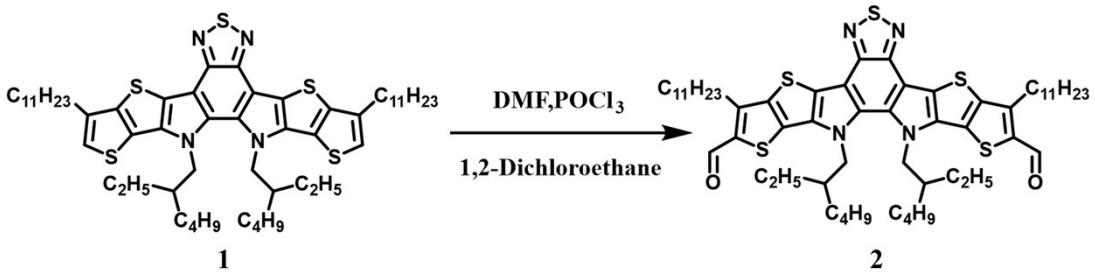

1 2

Scheme. S1 Synthetic route of compound **2**.

1.6 mL of 1,2-dichloroethane and 0.16 mL of N,N-dimethylformamide were mixed and cooled in an ice bath for 10 minutes, followed by the addition of 0.4 mL of phosphorus oxychloride ($POCl_3$) and reaction for 2 hours. Then, 100 mg (0.1 mmol) of TPB was dissolved in 5 mL of 1,2-dichloroethane, and the resulting solution was added to the aforementioned mixture, which was subsequently heated to reflux at 65 °C. After extraction and concentration, the product was purified by silica-gel column chromatography using petroleum ether/dichloromethane (2:1) as eluent to afford solid compound **2** (100.9 mg, 95% yield).

^{1}H NMR (400 MHz, Chloroform-*d*) δ 10.14 (s, 1H), 4.63 (dd, *J* = 7.9, 2.7 Hz, 2H), 3.20 (t, *J* = 7.7 Hz, 2H), 1.97 (dt, *J* = 29.9, 6.9 Hz, 4H), 1.47 (t, *J* = 7.8 Hz, 3H), 1.27 (d, *J* = 9.4 Hz, 15H), 1.04 (s, 2H), 0.92 (s, 3H), 0.87 (t, *J* = 6.8 Hz, 6H), 0.63 (dtd, *J* = 23.4, 7.2, 2.6 Hz, 7H).

Synthesis of (E)-12,13-bis(2-ethylhexyl)-10-(3-oxoprop-1-en-1-yl)-3,9-diundecyl-12,13-dihydro-[1,2,5]thiadiazolo[3,4-e]thieno[2'',3'':4',5']thieno[2',3':4,5]pyrrolo[3,2-g]thieno[2',3':4,5]thieno[3,2-b]indole-2-carbaldehyde(3)

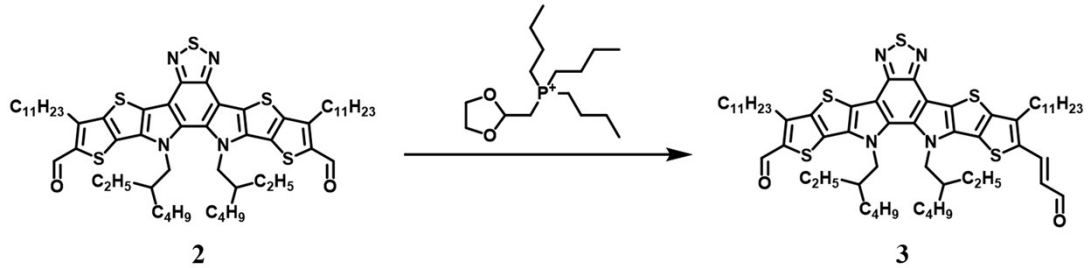

2 3

Scheme. S2 Synthetic route of compound **3**.

Compound **2** (100 mg, 0.1 mmol), Tributyl(1,3-dioxolan-2-ylmethyl)phosphonium bromide (40.6 mg, 0.11 mmol), sodium hydride (NaH) and tetrahydrofuran (THF) were stirred at room temperature for 16 hours. Subsequently, dilute hydrochloric acid was added, and the mixture was further reacted at room temperature for 4–5 hours. After extraction and concentration, the product was purified by silica-gel column chromatography using petroleum ether/dichloromethane (1:2) as the eluent to afford solid Compound **3** (58 mg, 57% yield).

^{1}H NMR (400 MHz, Chloroform-*d*) δ 10.14 (s, 1H), 9.71 (d, *J* = 7.6 Hz, 1H), 7.78 (d, *J* = 15.3 Hz, 1H), 6.53 (dd, *J* = 15.3, 7.6 Hz, 1H), 3.19 (d, *J* = 7.7 Hz, 2H), 2.99 (d, *J* = 7.8 Hz, 2H), 1.75 – 1.59 (m, 9H), 1.51 (s, 8H), 1.43 (s, 6H), 1.36 (s, 25H), 1.26 (d, *J* = 2.9 Hz, 37H), 0.99 – 0.92 (m, 12H), 0.92 – 0.85 (m, 27H), 0.85 – 0.75 (m, 12H), 0.71 – 0.56 (m, 16H).

Synthesis of BTP-1V-4F

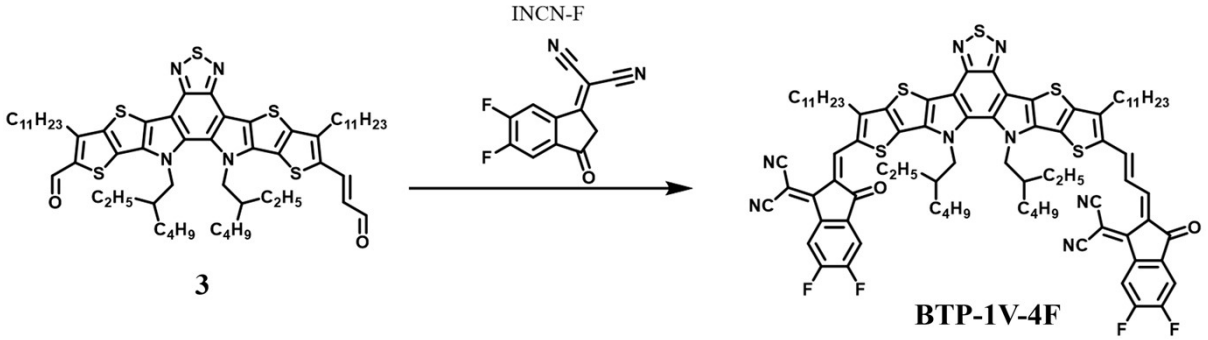

Scheme. S3 Synthetic route of BTP-1V-4F.

Compound **3** (60 mg, 0.057 mmol) and INCN-F (52.5 mg, 0.228 mmol) were dissolved in 10 mL of chloroform. Then, 0.4 mL of pyridine was added to the resulting solution, and the mixture was stirred at room temperature overnight. After extraction and concentration, the crude product was subjected to silica gel column chromatography using petroleum ether/dichloromethane (1:2) as the eluent, affording a deep blue solid (36.6 mg, 43% yield).

^{1}H NMR (400 MHz, Chloroform-*d*) δ 9.16 (d, *J* = 3.2 Hz, 1H), 8.70 – 8.56 (m, 1H), 8.56 – 8.46 (m, 2H), 7.76 – 7.65 (m, 3H), 4.75 (d, *J* = 8.2 Hz, 2H), 4.68 (d, *J* = 8.0 Hz, 2H), 3.24 (t, *J* = 7.9 Hz, 2H), 3.03 (t, *J* = 7.8 Hz, 2H), 2.13 – 2.03 (m, 2H), 1.88 (d, *J* = 7.2 Hz, 3H), 1.56 (s, 9H), 1.49 – 1.44 (m, 2H), 1.38 – 1.23 (m, 28H), 0.94 (dt, *J* = 62.6, 6.9 Hz, 20H), 0.78 – 0.61 (m, 11H).

Synthesis of BTP-1V-4Cl

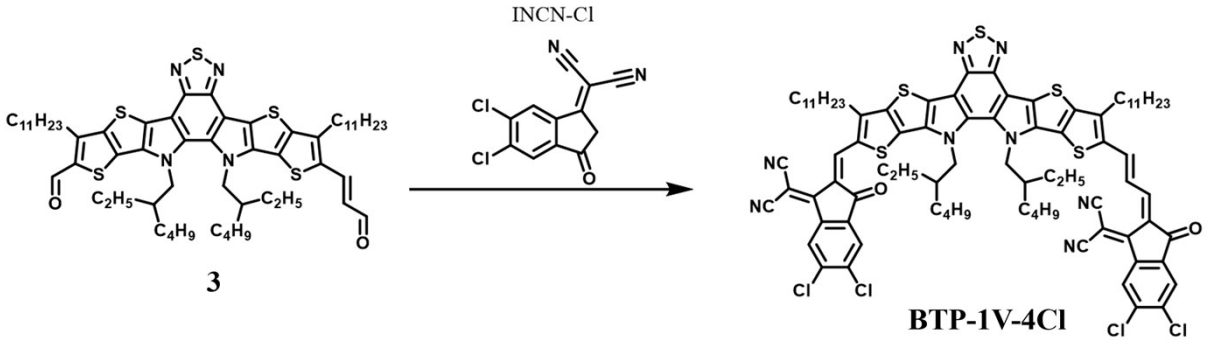

Scheme. S4 Synthetic route of BTP-1V-4Cl.

Compound **3** (47 mg, 0.04 mmol) and INCN-Cl (42 mg, 0.16 mmol) were dissolved in 10 mL of chloroform. Then, 0.25 mL of pyridine was added to the resulting solution, and the mixture was stirred at room temperature overnight. After extraction and concentration, the crude product was subjected to silica gel column chromatography using petroleum ether/dichloromethane (1:2) as the eluent, affording a deep blue solid (63 mg, 91% yield).

^{1}H NMR (400 MHz, Chloroform-*d*) δ 9.17 (d, *J* = 3.4 Hz, 1H), 8.78 (d, *J* = 8.9 Hz, 2H), 8.65 (dd, *J* = 14.2, 11.7 Hz, 1H), 8.52 (d, *J* = 11.7 Hz, 1H), 7.96 (d, *J* = 9.8 Hz, 2H), 7.73 (d, *J* = 14.2 Hz, 1H), 4.76 (d, *J* = 7.8 Hz, 2H), 4.68 (d, *J* = 7.9 Hz, 2H), 3.23 (t, *J* = 7.9 Hz, 2H), 3.03 (t, *J* = 7.8 Hz, 2H), 1.87 (d, *J* = 7.4 Hz, 4H), 1.35 (d, *J* = 15.0 Hz, 13H), 1.29 (s, 6H), 1.29 – 1.26 (m, 19H), 1.26 (s, 29H), 1.03 (s, 13H), 0.87 (d, *J* = 6.3 Hz, 10H), 0.84 (d, *J* = 7.1 Hz, 7H), 0.79 – 0.71 (m, 7H), 0.67 (dd, *J* = 7.2, 5.2 Hz, 7H).

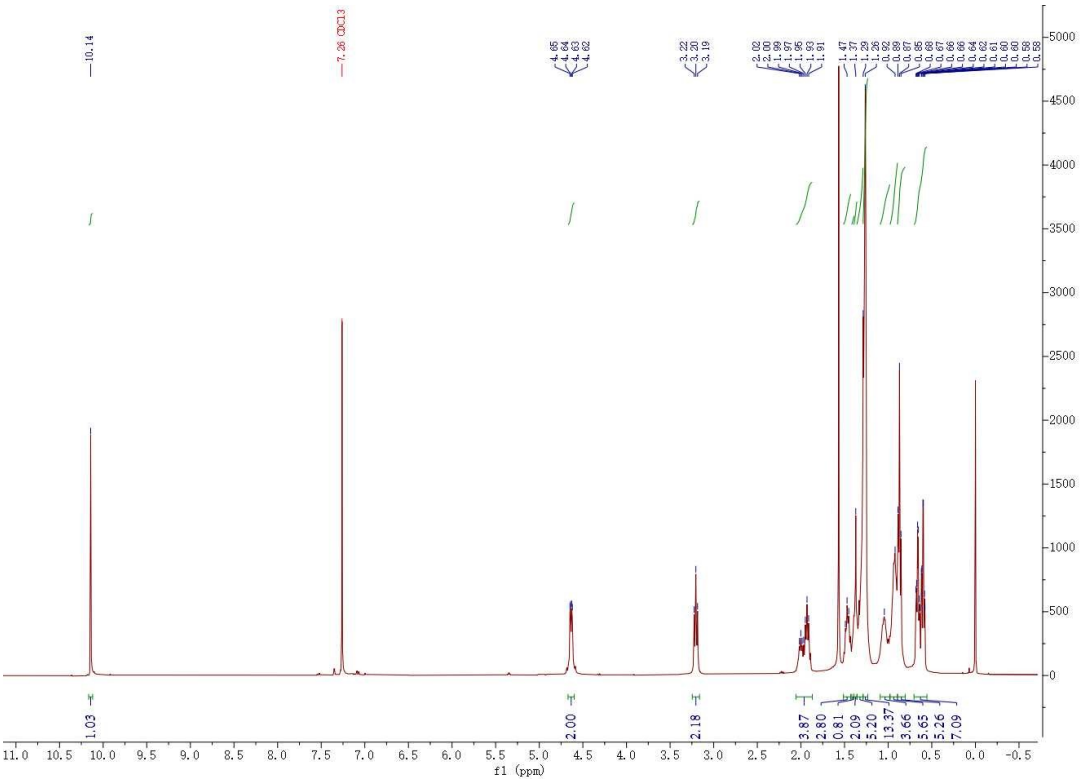

Figure S1. 1H NMR spectrum of compound 2 in CDCl3.

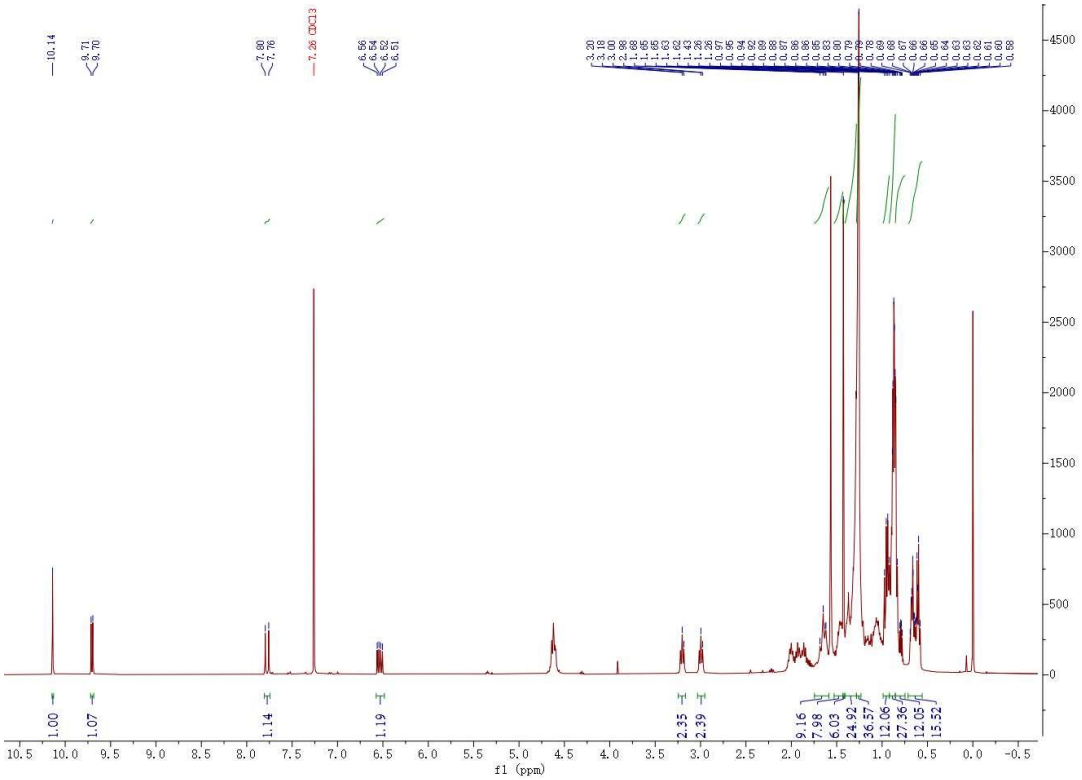

Figure S2. 1H NMR spectrum of compound 3 in CDCl3.

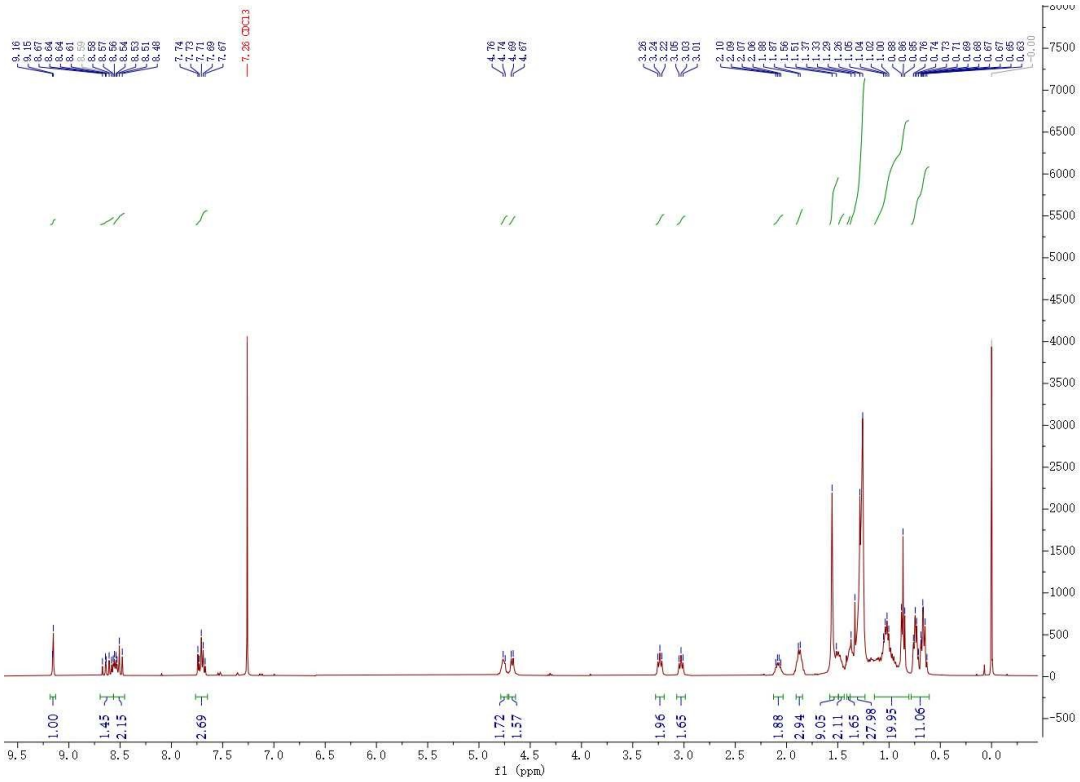

Figure S3. 1H NMR spectrum of BTP-1V-4F in CDCl3.

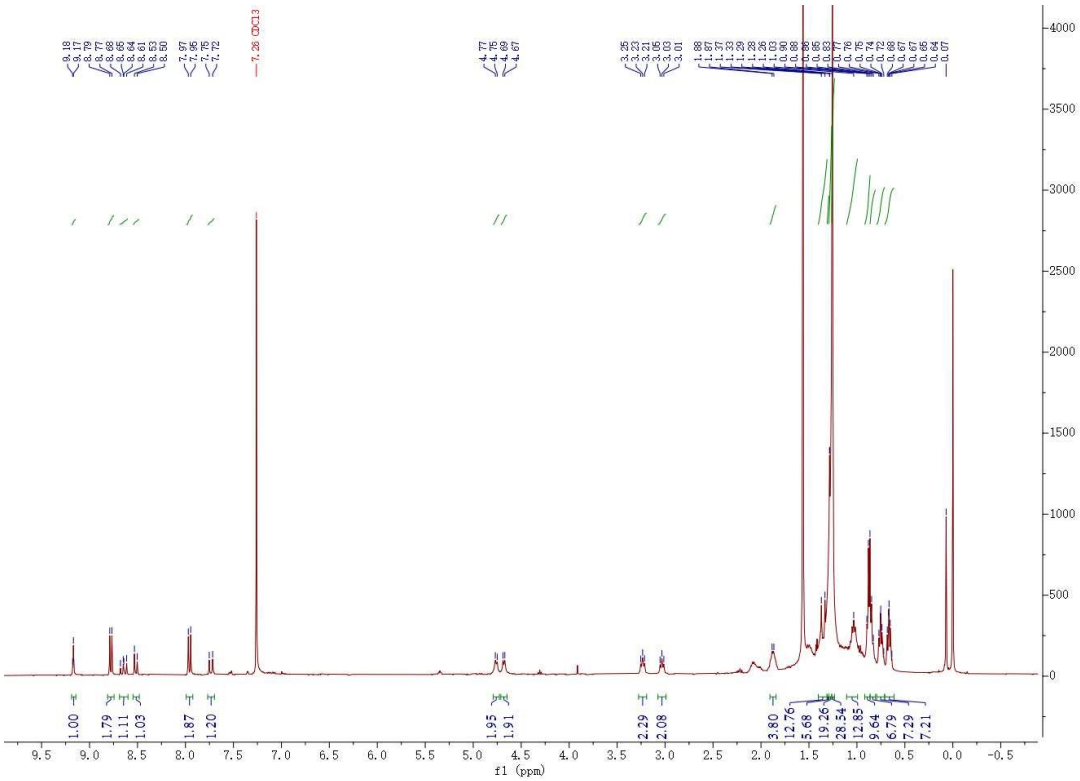

Figure S4. 1H NMR spectrum of BTP-1V-4Cl in CDCl3.

Device fabrication

OSC devices

The conventional device structure of ITO/PEDOT:PSS/Active layer/PDINN/Ag is used to construct the OSCs devices of the blends. The residual organic matter on the surface of the patterned indium tin oxide (ITO, about 15 Ω square^{-1}) glass substrates was ultrasonically cleaned with a cleaning solution, and then the cleaning solution was removed with deionized water. Next, the ITO conductive glass was ultrasonically cleaned with acetone and isopropyl alcohol in turn, and each step was ultrasonically cleaned for about 20 minutes. After drying, the cleaned ITO conductive glass was treated twice with oxygen plasma for 100 seconds each time before spinning and coating the hole transport layer (PEDOT:PSS). The PEDOT:PSS filtered with 0.45 μm PES is spin-coated on ITO at 4000 rpm for 30s and annealed at 155 °C for 15 min. Transfer the annealed ITO to the glove box with nitrogen atmosphere. The donor: acceptor blends solution with a weight ratio of 1:1.2 were dissolved in the chloroform (CF), in which the concentration is 16 mg/mL in total, with 1-chloronaphthalene (0.5–1.5 vol %) as the additive. Then the blend solution was stirred under 40 ˚C for 2 hours to mix intensively in a nitrogen-filled glove box. The blend 4 solution was spin-casted at 2700 rpm for 30 s onto the PEDOT:PSS films followed by a thermal annealing of 100 °C for 10 min. Then, the prepared PDINN solution (1 mg PDINN and 1 ml methanol were mixed and stirred for 1 hours) was spin-coated onto the active layers at 3000 rpm for 20 s. Finally, in the vacuum condition of 10^{-4} Pa, 80 nm Ag was deposited by thermal evaporation with a shadow mask of 0.0936 cm^{-2}.

OPD devices

The OPDs were fabricated with the device structure of ITO/ZnO/photoactive layer/MoO_3/Ag. The cleaned ITO substrates were dried using high purity nitrogen and treated with oxygen plasma for 100 seconds. ZnO precursor solution was prepared by dissolving zinc acetate dehydrate 100 mg into 2 mL 2-methoxyethanol with 28 uL ethanolamine, and was spin coated on ITO substrates at 4000 rpm for 60 s. Then, ITO substrates coated with ZnO films were heated at 200 °C for 30 min in air and were transferred into the nitrogen-filled glove box to fabricate the active layers. Donors and acceptors blended with the mass ratio of 1:1.2 and the concentration of 22 mg/mL in total, were dissolved in CF solvent and stirred about 3 hours at 40 ˚C. Then, the solutions were spin coated on the ZnO modified ITO substrates and then thermal annealed at 100 °C for 10 min. The thickness of the blend film was controlled at about 200 nm. The thickness of films was measured by a contact

profilometer (Dektak 6 M, Bruker). Finally, 8 nm MoO_3 and 80 nm Ag were deposited under the 2.0×10^{-4} Pa vacuum condition.

Characterization

NMR spectra were recorded on Bruker AVANCE III 400 MHz spectrometer at 298K.

Cyclic voltammetry (CV) measurements were performed on a CHI660D electrochemical workstation, equipped with a three-electrode cell consisting of a platinum working electrode, a saturated calomel electrode (SCE) as reference electrode and a platinum wire counter electrode. CV measurements were carried out in anhydrous acetonitrile containing 0.1 M n-Bu_4NPF_6 as a supporting electrolyte under an argon atmosphere at a scan rate of 100 mV s^{-1} with Fc/Fc^+ as the reference. The HOMO and LUMO of the objective compounds are calculated according to the following equations:

$$HOMO = -[E_{ox}^{onest} + 4.40]$$

$$LUMO = -[E_{red}^{onest} + 4.40]$$

Where E_{ox}^{onest} and E_{red}^{onest} are the onset of oxidation potential and reduction potential, respectively.

The absorption spectrum was recorded using a Hitachi U-4100 UV-Vis scanning spectrophotometer. Temperature-dependent absorption spectra were recorded on a Hitachi U-4100 UV-Vis scanning spectrophotometer. In situ absorption spectra were measured on PerkinElmer UV-Vis spectrometer, model Lambda 750. All film samples were spin-cast on quartz glass.

The ground-state geometries of NFAs-BTP molecules were fully optimized with DFT method under B3LYP/6-31G (d, p) level.

The photoluminescence (PL) spectra and time-resolved photoluminescence (TRPL) spectra were recorded by FLS1000 Edinburgh steady state and transient fluorescence spectrometer.

Atomic Force Microscope (AFM) images were obtained using a multifunctional scanning probe microscope (Oxford Cypher ES). All film samples were spin-cast on ITO substrates.

Transmission electron microscope (TEM) images were obtained by using a HITACHI HT-7800 electron microscope with an acceleration voltage of 80kV.

Grazing incidence wide-angle X-ray scattering (GIWAXS) were measured at the synchrotron radiation center of Shanghai light source. All film samples were spin-cast on silicon wafer treated by plasma. The grazing angle is selected at 0.12°–0.16°.

The Contact Angle (CA) were recorded by CSCDIC-200S. After the target material was prepared on ITO glass, the CA was tested using water and diiodomethane as the medium, respectively. The surface tension and interfacial tension are calculated based on the polarity and dispersion components of the two mediums. The calculation formula is as follows:

$$\gamma_{water}(1+\cos\theta_{water}) = \frac{4\gamma_{water}^{d}\gamma^{d}}{\gamma_{water}^{d}+\gamma^{d}} + \frac{4\gamma_{water}^{p}\gamma^{p}}{\gamma_{water}^{p}+\gamma^{p}}$$

$$\gamma_{DIM}(1+\cos\theta_{water}) = \frac{4\gamma_{DIM}^{d}\gamma^{d}}{\gamma_{DIM}^{d}+\gamma^{d}} + \frac{4\gamma_{DIM}^{p}\gamma^{p}}{\gamma_{DIM}^{p}+\gamma^{p}}$$

$$\gamma^{total} = \gamma^{d} + \gamma^{p}$$

$$\gamma_{A-B} = \gamma_{A} + \gamma_{B} - \frac{4\gamma_{A}^{d}\gamma_{B}^{d}}{\gamma_{A}^{d}+\gamma_{B}^{d}} + \frac{4\gamma_{A}^{p}\gamma_{B}^{p}}{\gamma_{A}^{p}+\gamma_{B}^{p}}$$

where θ is the contact angle; γ^{total} is the surface tension;γ_i is the surface tension of the medium (water, diiodomethane); γ_i^d and γ_i^p is the dispersion component and the polarity component; γ_{A-B} is the interfacial tension between materials A and B; $\gamma_A$and γ_B are materials Surface tension of materials A and B.

The Flory-Huggins interaction number (χ) characterizing the blending properties of the donor and acceptor materials is based on the formula:

$$\chi = \kappa(\sqrt{\gamma_D} - \sqrt{\gamma_A})^2$$

where κ is constant; γ_D and γ_A are the surface tensions of the donor and acceptor materials, respectively.

The current density-voltage (*J–V*) curves of all the fabricated solar cells were measured under an illumination of AM 1.5G (100 mW cm^{-2}) using a Keithley 2400 and an XES-40S2 (SANEI ELECTRIC Co., Ltd) solar simulator (AAA grade, 70×70 mm^2 photo beam size).

The dark *J–V* curves (J_d) of OPD devices were measured using a Keysight B2985B Electrometer in dark condition. The test temperature in the laboratory is room temperature, which is about 25 ˚C.

The External quantum efficiency (EQE) and Responsivity (*R*) spectra were performed on PD-QE, Enlitech Co. Ltd. The light intensity at each wavelength was calibrated using a standard photovoltaic cell (Si and Ge detectors).

Frequency-dependent noise spectra were also performed on QE-PD, Enlitech Co. Ltd. The bias voltage is from 0 V to −1 V and the frequency is from 1 Hz to 10 kHz.

Linear dynamic range (LDR) was measured under a series of light intensities calibrated by an optical power meter.

Response speed. The response speed was characterized by the rise time (τ_r) and decay time (τ_d), defined as the time interval required for the photocurrent to increase from 10% to 90% and decrease from 90% to 10% of its maximum value, respectively. The response times were measured using a square-wave pulsed laser (850 nm) with a laser frequency of 20 kHz and an oscilloscope (Keysight MSO56B 5-BW-500).

Photoplethysmography (PPG) and the heart rate (HR) were calculated using a PPG pulse signal, and the test setup consists of an 850 nm LED light and the OPDs, which used an oscilloscope to read out the signal and then filtered it to obtain a clear pulse signal.

Hole mobilities and electron mobilities were measured via Space charge limited current (SCLC) method. The structure of hole-only device was Glass/ITO/PEDOT:PSS/Active layer/MoO_3/Ag (100 nm). The structure of electron-only device was Glass/ITO/ZnO/Active layer/PDINO/Ag (100 nm). The electron and hole mobilities were calculated by using the modified Mott–Gurney equation:

$$J = \frac{8}{9}\varepsilon_0\varepsilon_r r\mu\frac{V^2}{d^3}$$

where J is the current density, μ is the charge carrier mobility, ε_0 is the permittivity of free space, ε_r is the relative permittivity of the material, d is the thickness of the active layers, and V is the effective voltage. The effective voltage was obtained by subtracting the built-in voltage (V_{bi}) and the voltage drop (V_s) from the series resistance of the whole device except for the active layers from the applied voltage (V_{appl}), $V = V_{appl} - V_{bi} - V_s$. The mobility is calculated from the slope of the $J^{1/2}$–V curves.

Trap density (N_t) was estimate using the dark current−voltage (I−V) curves of electron-only devices with structure of ITO/ZnO/Active layer/PDINN/Ag were obtained by SCLC method as well according to Equation:

$$V_{TFL} = e\frac{N_{trap}}{2\varepsilon_0\varepsilon_r}L^2 \#(4)$$

where V_{TFL} is trap-filled-limit-voltage identified from trap-filling region of characteristics. ε_0 is dielectric constant of free space and ε_r is relative dielectric constant of active layers, usually as 3. L is film thickness, and e represents elementary charge.

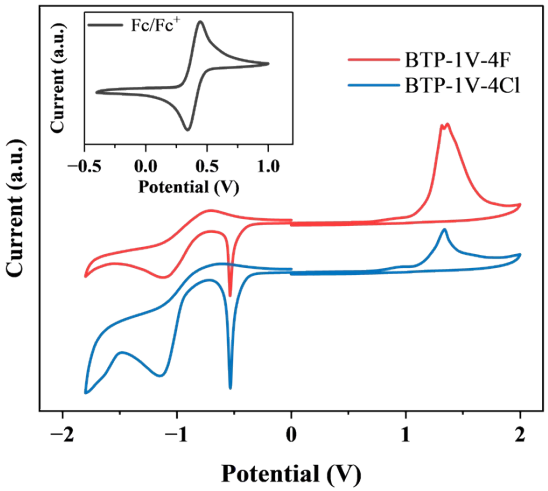

Figure S5. CV curves of BTP-1V-4F and BTP-1V-4Cl

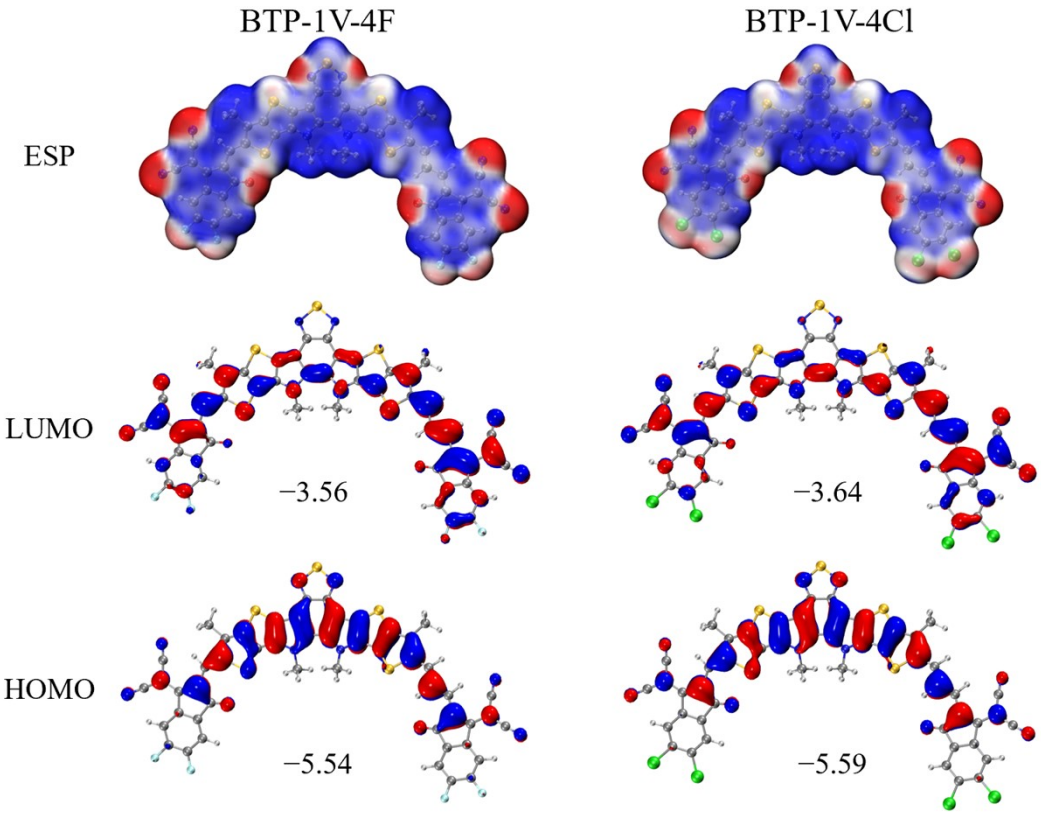

Figure S6. ESP maps and LUMO/HOMO of BTP-1V-4F and BTP-1V-4Cl calculated by DFT simulation calculation.

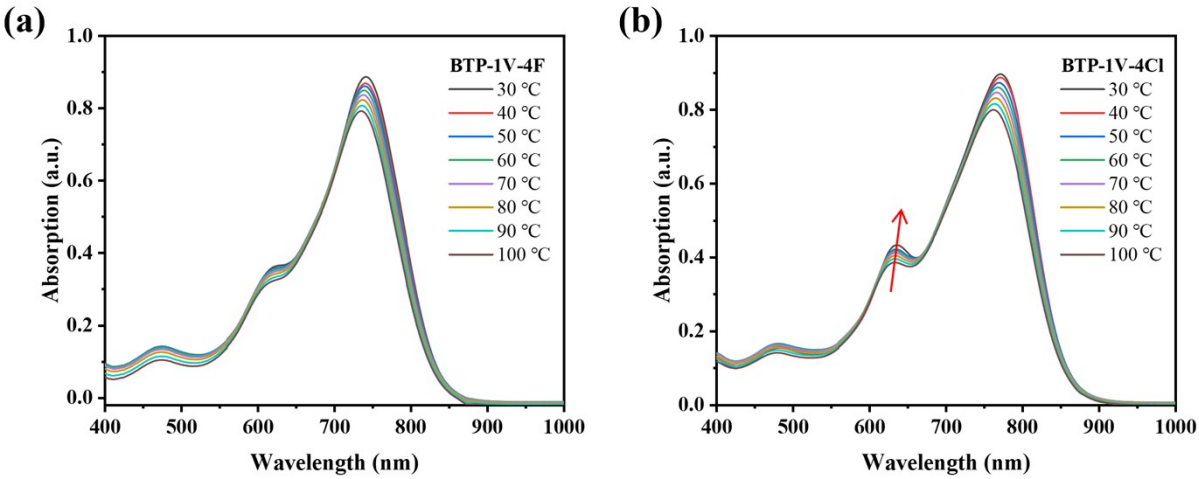

Figure S7. The temperature-dependent UV-vis absorption of (a) BTP-1V-4F and (b) BTP-1V-4Cl.

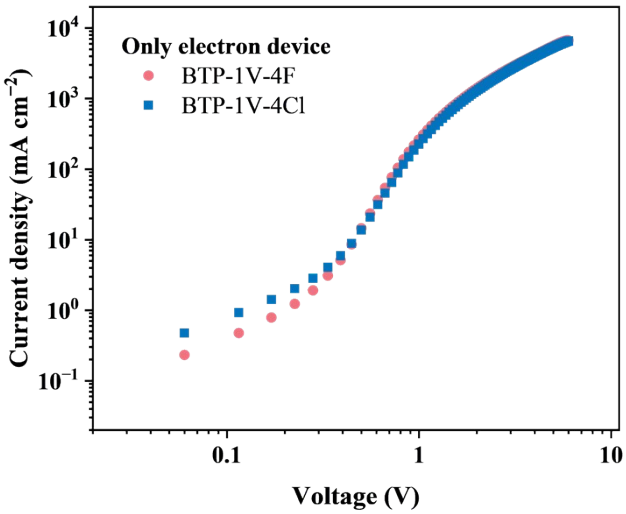

Figure S8. The electron mobilities of neat acceptor films.

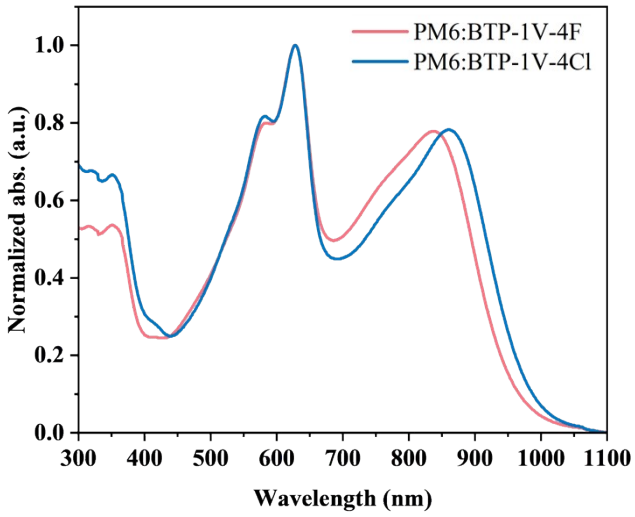

Figure S9. Normalized absorption of blend films.

Table S1. Photovoltaic parameters of BTP-1V-4F and BTP-1V-4Cl OSCs devices under different annealing conditions.

Active layer	Annealing	V_{OC} (V)	J_{SC} (mA cm^{-2})	FF (%)	PCE (%)
PM6:BTP-1V-4F	w/o	0.815	22.41	63.13	11.53
	TA	0.792	25.11	60.01	11.94
PM6:BTP-1V-4Cl	w/o	0.796	20.04	60.60	9.66
	TA	0.787	23.17	59.54	10.86

Table S2. Photovoltaic parameters of BTP-1V-4F and BTP-1V-4Cl OSCs devices under different donor/acceptor (D/A) ratio.

Active layer	D:A ratio	V_{OC} (V)	J_{SC} (mA cm^{-2})	FF (%)	PCE (%)
PM6:BTP-1V-4F	1:11	0.781	23.45	68.22	12.50
	1:1.2	0.788	24.01	69.36	13.13
	1:1.5	0.798	23.25	66.40	12.32
PM6:BTP-1V-4Cl	1:1	0.781	22.56	61.96	10.91
	1:1.2	0.784	21.94	65.40	11.25
	1:1.5	0.768	22.62	56.79	9.87

Table S3. Photovoltaic parameters of BTP-1V-4F and BTP-1V-4Cl OSCs devices with different additive concentrations.

Active layer	1-CN	V_{OC} (V)	J_{SC} (mA cm^{-2})	FF (%)	PCE (%)
PM6:BTP-1V-4F	w/o	0.792	25.11	60.01	11.94
	0.5 %	0.788	24.01	69.36	13.13
	1.0 %	0.789	17.73	72.56	10.15
	1.5 %	0.782	15.26	73.87	8.82
PM6:BTP-1V-4Cl	w/o	0.787	23.17	59.54	10.86
	0.5 %	0.784	21.94	65.40	11.25
	1.0 %	0.782	17.23	64.21	8.65
	1.5 %	0.782	17.19	63.49	8.53

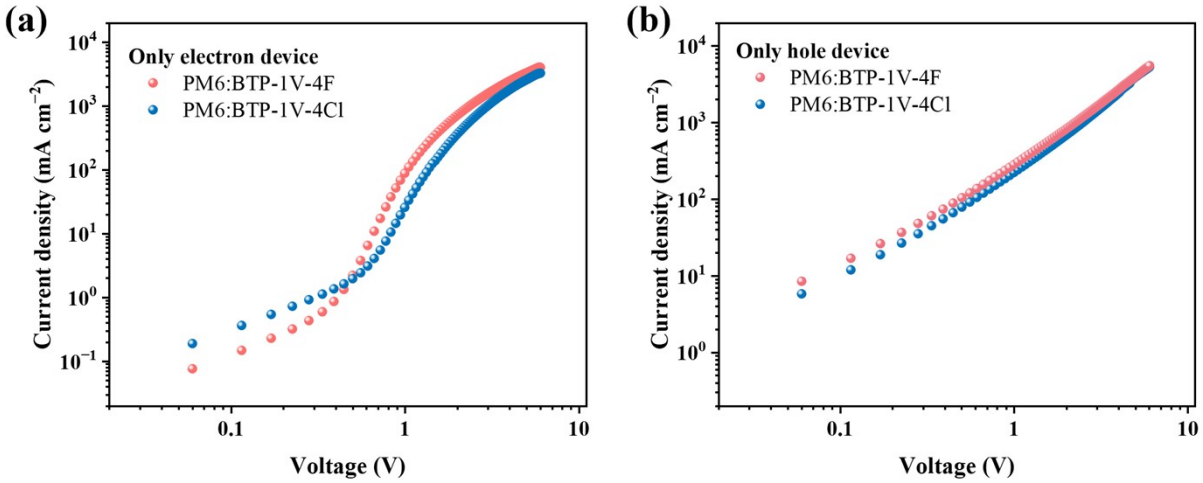

Figure S10. The hole and electron mobilities of BTP-1V-4F and BTP-1V-4Cl blend films

Table S4. The hole and electron mobilities of BTP-1V-4F and BTP-1V-4Cl blend films.

Active layer	μ_e (cm^2 V^{-1} s^{-1})	μ_h (cm^2 V^{-1} s^{-1})	μ_e/μ_h
PM6:BTP-1V-4F	5.56×10^{-4}	5.43×10^{-4}	1.02
PM6:BTP-1V-4Cl	3.57×10^{-4}	4.99×10^{-4}	0.72

Table S5. Charge dynamics parameters of BTP-1V-4F and BTP-1V-4Cl OSCs devices.

Active layer	P_{diss} (%)	P_{coll} (%)	α	n (kT/q)	N_t (cm^{-3})
PM6:BTP-1V-4F	97.23	86.32	0.98	1.13	1.31×10^{16}
PM6:BTP-1V-4Cl	96.10	82.14	0.97	1.29	2.06×10^{16}

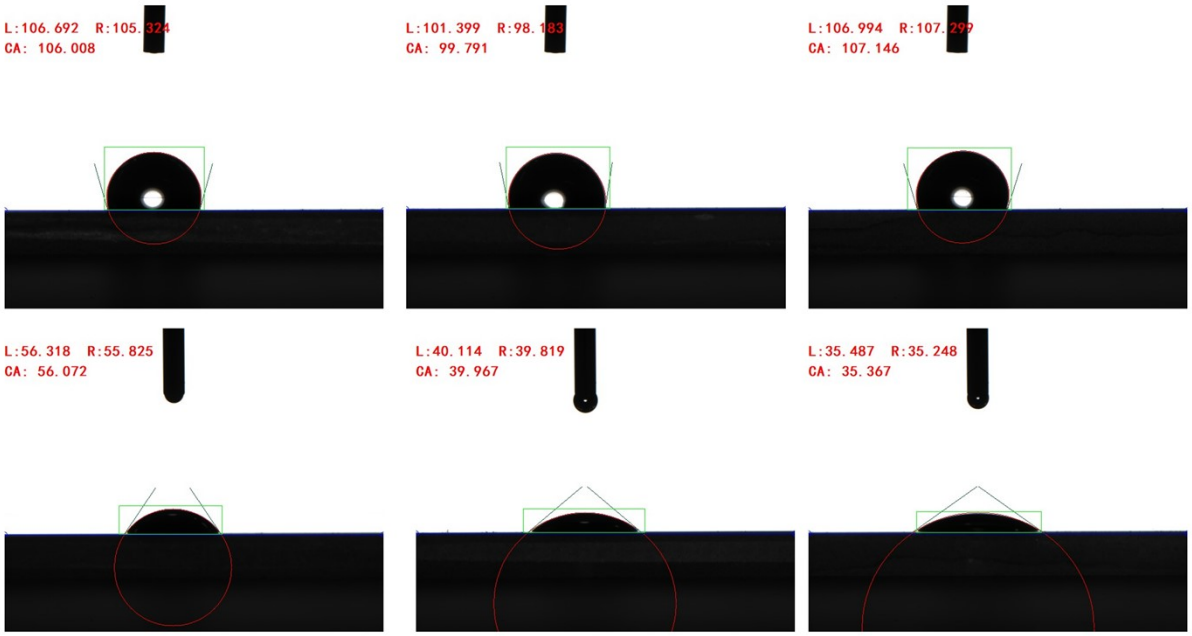

Figure S11. Contact angles of PM6, BTP-1V-4F and BTP-1V-4Cl neat films.

Table S6. Contact angle, surface energy and compatibility coefficient of PM6, BTP-1V-4F and BTP-1V-4Cl.

Films	θ_{H2O} (°)	θ_{CH2I2} (°)	γ_s (mN/m)	$\chi_{D,A}$ (κ)
PM6	106.008	56.072	33.404	-
BTP-1V-4F	99.791	39.967	42.725	0.57
BTP-1V-4Cl	107.146	35.367	49.471	1.57

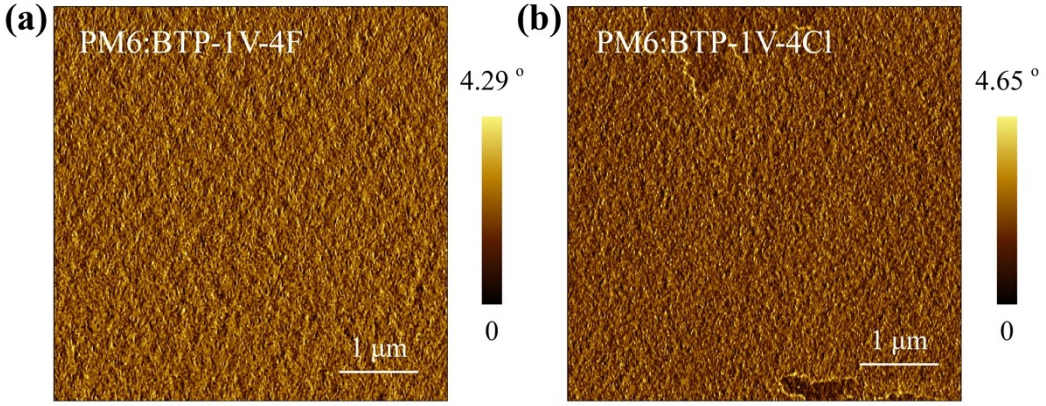

Figure S12. AFM phase images of PM6:BTP-1V-4F and PM6:BTP-1V-4Cl blend films.

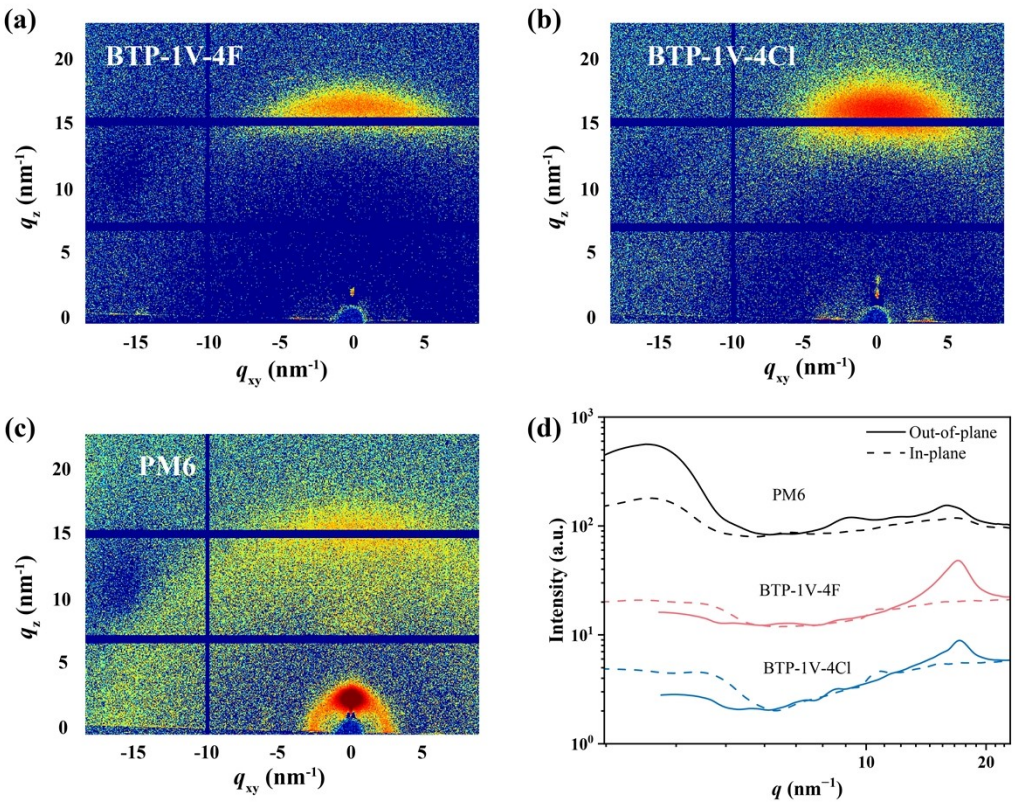

Figure S13. 2D GIWAXS pattern of (a) BTP-1V-4F, (b) BTP-1V-4Cl and (c) PM6 neat films. (d) 1D line profiles.

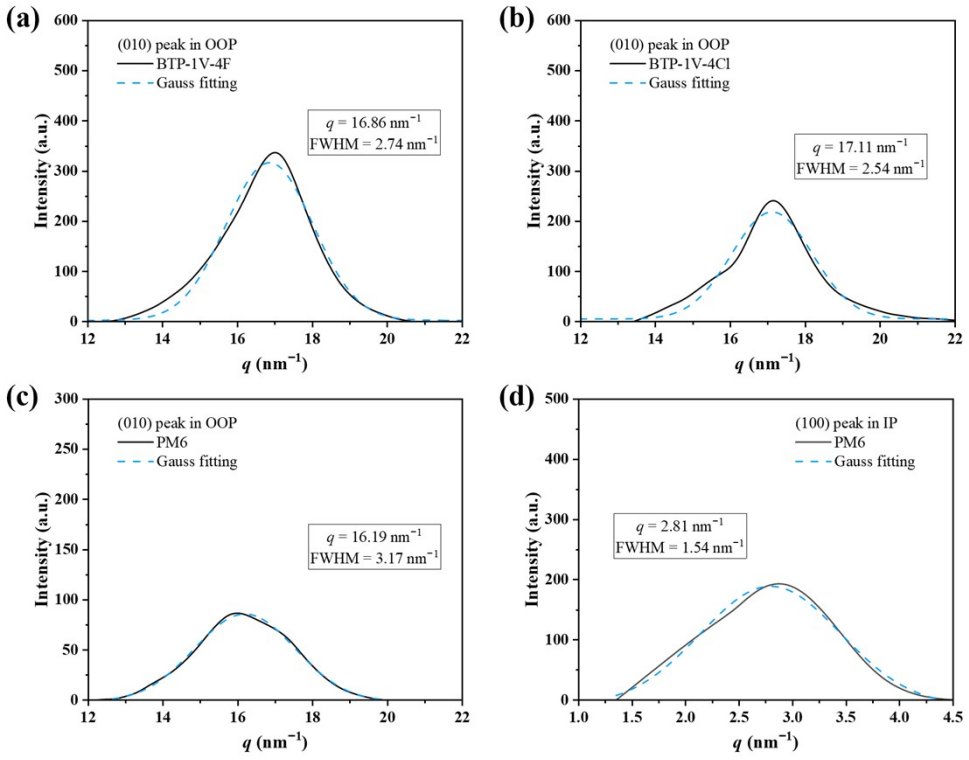

Figure S14. Gauss fitting for (010) peak in OOP direction or (100) peak in IP direction of neat films.

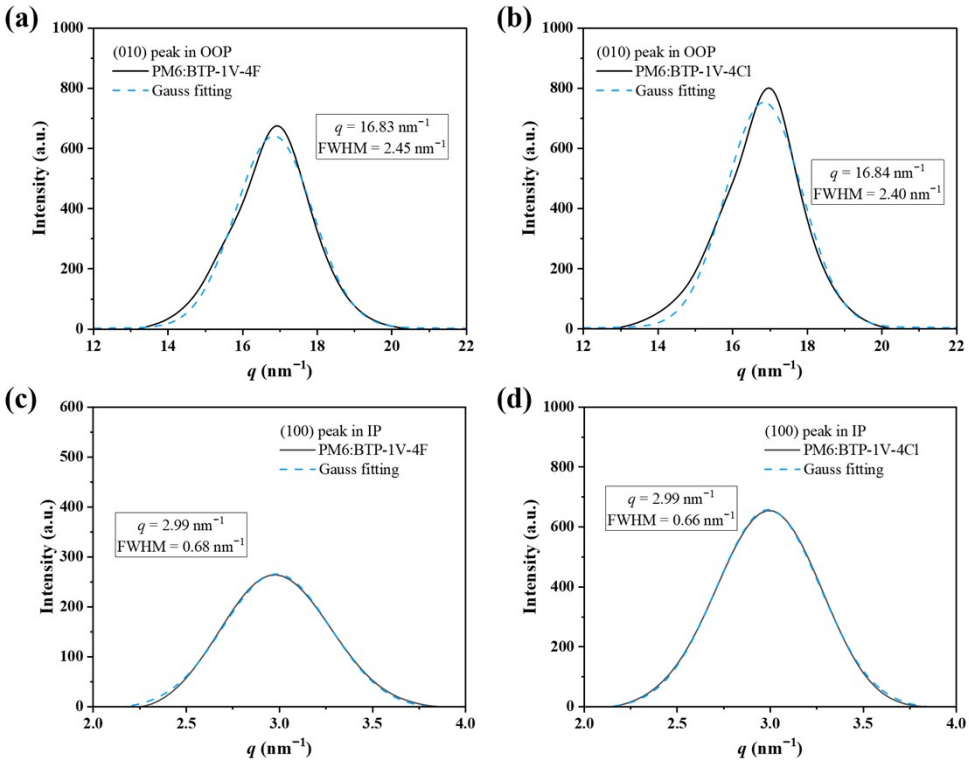

Figure S15. Gauss fitting for (010) peak in OOP direction or (100) peak in IP direction of PM6:BTP-1V-4F and PM6:BTP-1V-4Cl blend films.

Table S7. The detailed data of (100) peaks in IP direction of different films.

Films	(100) peak in IP			
	q (nm^{-1})	$d_{\pi\text{-}\pi}$ (Å)	FWHM (nm^{-1})	CCL (Å)
PM6	2.81	22.36	1.54	36.72
PM6:BTP-1V-4F	2.99	21.01	0.68	83.16
PM6:BTP-1V-4Cl	2.99	21.01	0.66	85.68

Table S8. The detailed data of (010) peaks in OOP direction of different films.

Films	(010) peak in OOP			
	q (nm^{-1})	$d_{\pi\text{-}\pi}$ (Å)	FWHM (nm^{-1})	CCL (Å)
PM6	16.19	3.88	3.17	17.84
BTP-1V-4F	16.86	3.73	2.74	20.64
BTP-1V-4Cl	17.11	3.67	2.54	22.26
PM6:BTP-1V-4F	16.83	3.73	2.45	23.08
PM6:BTP-1V-4Cl	16.84	3.73	2.40	23.56

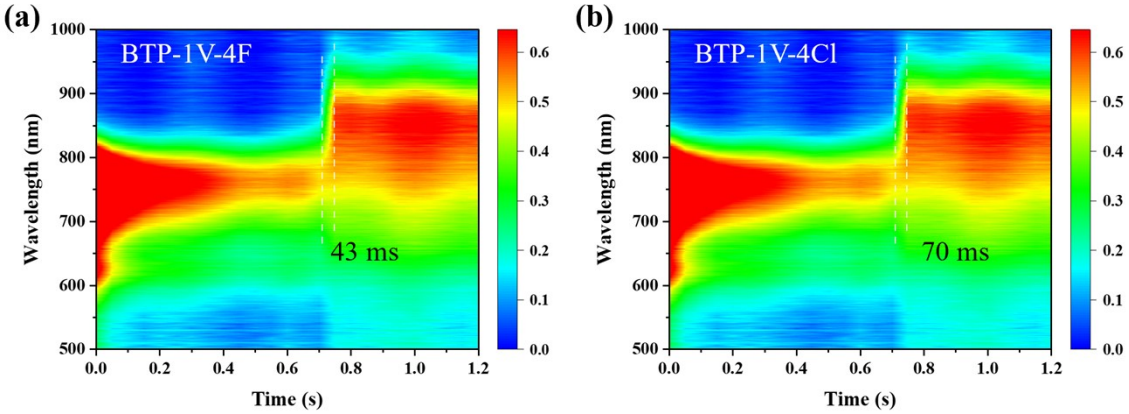

Figure S16. In-situ absorption spectra of (a) BTP-1V-4F and (b) BTP-1V-4Cl.

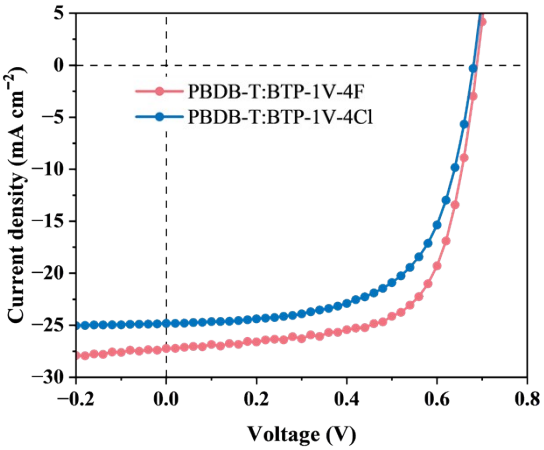

FigureS17. *J–V* curves of PBDB-T:BTP-1V-4X based OSCs.

Table S9. Photovoltaic parameters of PBDB-T:BTP-1V-4X based OSCs

Active layer	V_{OC} (V)	J_{SC} (mA cm^{-2})	FF (%)	PCE (%)
PBDB-T:BTP-1V-4F	0.688	27.28	66.58	12.50
PBDB-T:BTP-1V-4Cl	0.680	24.81	62.37	10.54

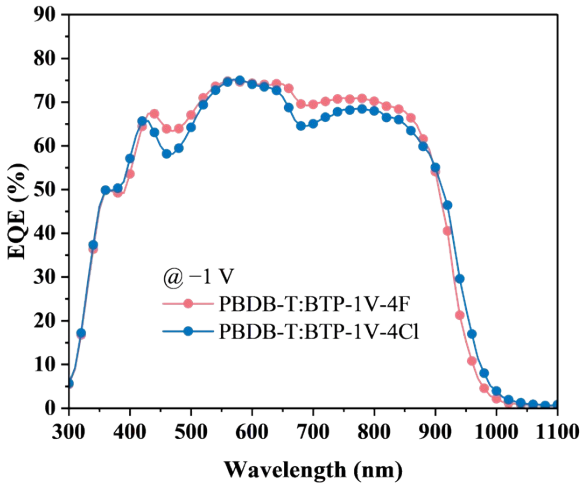

Figure S18. EQE spectra of PBDB-T:BTP-1V-4F and PBDB-T:BTP-1V-4Cl OPDs at −1 V bias.

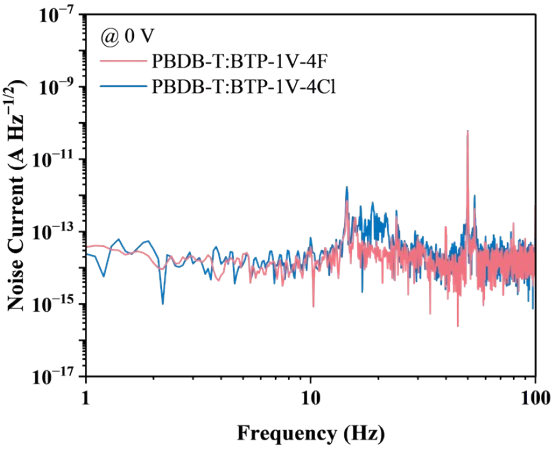

Figure S19. Frequency noise density spectral at 0 V bias.

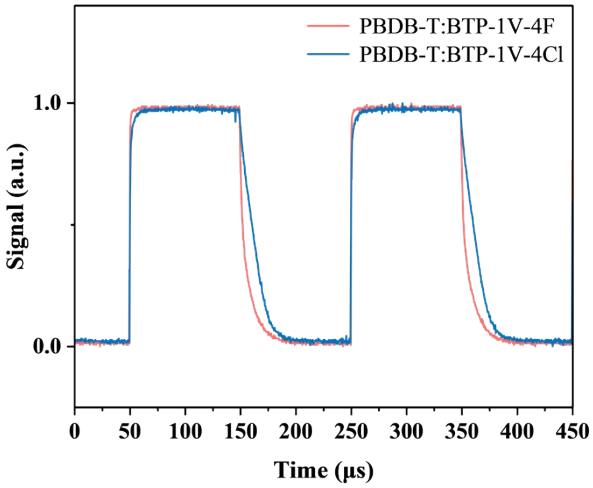

Figure S20. Response time of PBDB-T:BTP-1V-4F and PBDB-T:BTP-1V-4Cl OPDs. The laser wavelength is 850 nm.